Investigation of buried EUV mask defect printability using actinic inspection and fast simulation

Chris H. Clifford*[1], Tina T. Chan[1], Andrew R. Neureuther[1], Kenneth A. Goldberg[2], Iacopo Mochi[2], Ted Liang[3]

[1]Department of Electrical Engineering and Computer Sciences, University of California, Berkeley, CA 94720
[2] Lawrence Berkeley National Laboratory, 1 Cyclotron Road, Berkeley, CA 94720
[3] Intel Corp., 2200 Mission College Blvd., Santa Clara, CA 95054

ABSTRACT

The fast simulator RADICAL and the Actinic Inspection Tool (AIT) are used in advance of availability of high volume manufacturing quality exposure tools, resists, and masks to assess the expected defect printability levels in production conditions. AIT images are analyzed to qualitatively demonstrate general trends in defect printability: defects smaller than 0.5nm tall on the multilayer surface can cause an unacceptable critical dimension (CD) change, CD change increases for taller defects, and defect printability varies asymmetrically through focus. RADICAL is used to derive quantitative limits for defect size and demonstrate the effects of focus and illumination for 22nm and 16nm dense lines. For 22nm dense lines at best focus a 0.8nm tall defect causes a 10% CD change. For 16nm lines a 0.4nm tall defect causes a 10% CD change. The CD is shown to be more sensitive to buried defects out of focus, but less sensitive to defects in focus if annular or dipole illumination is used.

Keywords: actinic EUV inspection, fast simulation, buried defect, EUV mask

1. INTRODUCTION

As the research and development of extreme ultraviolet (EUV) lithography continues, the problem of mask defects is increasing in importance [1]. This is because there is no commercial inspection tool capable of detecting buried defects on a patterned EUV mask, the defectivity of EUV mask blanks does not yet meet the current high volume manufacturing requirements, and it is not clear that the current specifications in the ITRS roadmap for maximum allowable defect sizes are adequate. This paper will address the issues of mask inspection, by showing results of the actinic inspection tool, and minimum defect size, by simulating the effects of buried defects near 22nm and 16nm dense lines. The data from the AIT will show its capabilities and also illustrate general trends of defect printability. RADICAL simulation will confirm these trends and expand upon them with quantitative analysis.

Actinic Inspection Tool

The AIT is a direct CCD actinic (EUV-wavelength) EUV mask inspection tool [2]. It employs a bending magnet at the Advanced Light Source synchrotron at Lawrence Berkeley National Laboratory as its source and uses a Fresnel zone plate lens to project a high-magnification image with numerical aperture values that emulate current and projected EUV lithography printing tools. Bitmap aerial images recorded by the AIT are suitable for direct comparison with bitmaps from simulation.

All AIT images shown in this work were recorded in December 2008. The zoneplate producing a 4x equivalent NA of 0.3 was used. The illumination of the AIT is highly coherent, and is modeled using a sigma value of 0.1. The through focus images are recorded by slightly varying the wavelength, rather than physically moving any component of the system [3].

* chris@eecs.berkeley.edu; phone: (651) 238-9628

Photomask Technology 2009, edited by Larry S. Zurbrick, M. Warren Montgomery,
Proc. of SPIE Vol. 7488, 74882H · © 2009 SPIE · CCC code: 0277-786X/09/$18 · doi: 10.1117/12.829716

RADICAL

A new simulator, RADICAL (Rapid Absorber Defect Interaction Computation for Advanced Lithography) described in in [4], can simulate EUV masks with buried defects and absorber features three orders of magnitude faster than the finite difference time domain (FDTD) using two orders of magnitude less memory. This speedup is accomplished by simulating the absorber features and defective multilayer separately using simulation methods optimized for each. The absorber layout simulator runs without regard for the multilayer geometry and the multilayer simulator runs without regard for the absorber layout. This modularity makes the fast and accurate simulation of a large mask area containing buried defects possible.

Programmed Defect Mask

All AIT inspections were done on the same programmed defect mask in which 48nm high posts with a square base on a substrate were over-coated with a multilayer. The width of the posts was varied. It turns out that the smoothing process used for the multilayer deposition produced defects which all have between a 50 and 60 nm full width half max (FWHM) diameter and heights ranging up to 8nm [5]. It was shown in [6] that the most critical dimension of an over-coated buried defect is the surface height. Therefore, that will be the only dimension mentioned in this paper. The substrate and surface sizes of all the defects on the mask is given in Table 1. This mask has only substrate bumps, not pits. Therefore, bumps will be the focus of this work.

Buried Width	Buried Height	Surface Width (FWHM)	Surface Height
100	48	60	8
95	48	59	7
90	48	58	6.2
85	48	56	5.3
80	48	55	4.4
75	48	54	3.5
70	48	53	2.6
65	48	52	1.7
60	48	51	0.8

Table 1. Defect sizes for the programmed defect mask. Buried defects are boxes on the substrate with a square base and constant height. The surface defects are the result of the multilayer smoothing and are roughly Gaussian shaped.

2. DEFECT PRINTABILITY MEASURED BY AIT

Buried defect data from the AIT was first compared to RADICAL in [7]. This work showed how aberrations in the AIT were extracted by comparison to RADICAL simulations of isolated defects. It also showed a good match between RADICAL and the AIT for the aerial image of a defect near a feature through focus. This shows that RADICAL accurately predicts the magnitude and phase of the field reflected by an EUV mask with a buried defect. This work has continued since that publication, and new results from the AIT are presented in this paper which demonstrate a few important effects which will be studied in detail for the 22nm and 16nm node through simulation.

For all experiments and simulations in this work, the critical dimension (CD) of the *space* will be measured. The space is defined as the bright area between two dark lines. The space CD is measured because a defect normally affects the edges of the two lines near it. Therefore, measuring just one line edge is misleading.

Figure 1 shows the space CD change for a 250nm dense line space pattern. There are a few important things to note. The first is that even the 0nm defect has some CD change. This is simply a background uncertainty level, due to noise in the AIT system and mask roughness both on the multilayer surface and absorber line edges. A measurement must be above this level, about 15nm at best focus, for it to be meaningful. The CD change for the 0.8nm defect is above this level. That means that a 0.8nm tall surface defect can be detected by the AIT. This will be shown below to be the approximate size of the maximum allowable defect for 22nm dense lines on the wafer. The effect of focus is also obvious in Figure 1. As the focus gets more negative, the CD change due to the defect gets larger. The inversion of aerial image intensity through focus is discussed in detail for isolated defects in [7], so this effect from defects near

features is not surprising. The effect of positive focus is not as obvious in Figure 1. The values on the right side of Figure 1 jump around a lot more than the left side. The reason for this is clear in Figure 2. The phase of the defect, combined with the positive focus and high coherence of the illumination, causes a bright spot on the side of the line. This causes a bright protrusion from the line centered between two dark intrusions, which makes the CD change difficult to define.

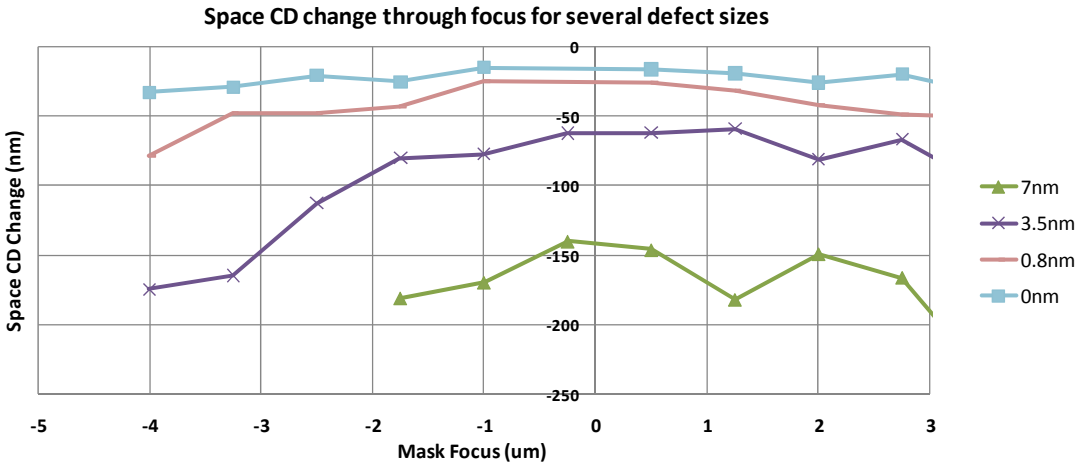

Figure 1. Space CD (mask scale) change through focus for several defect sizes. All defects are 50- 60nm FWHM and centered in the space between dense 250nm absorber lines 55nm from the edge of the absorber. The labels for each curve are surface height.

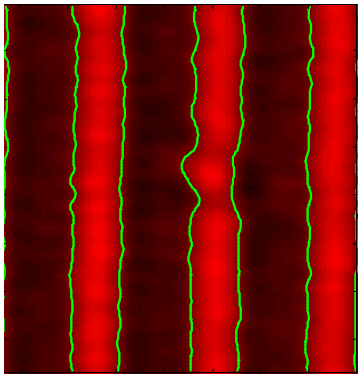

Figure 2. AIT image of a buried defect with a surface height of 5.3nm on the edge of an absorber line for focus = 4um.

Figure 3 shows the CD change as a function of surface defect height. This clearly shows, that the larger defects result in larger CD changes. It also shows again that more negative defocus causes a larger CD change. There is an obvious correlation in unexpected behavior between the CD changes for a given defect size at each focus value. For example, the CD actually increases from the 3.5nm to 4.4nm tall defects. This is likely because the absorber near this defect is smaller than nominal due to variability in the mask fabrication. But, the general trend is that larger defects cause larger CD changes.

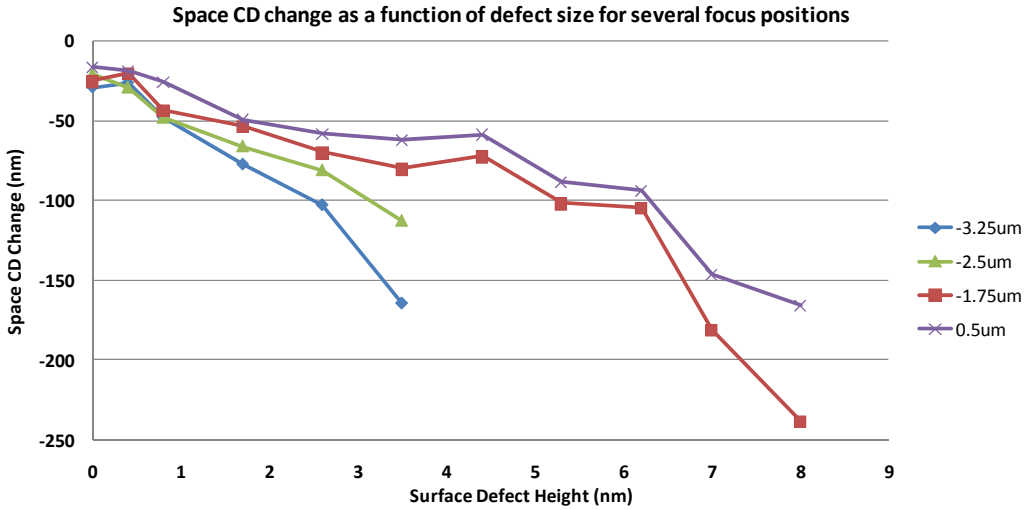

Figure 3. Space CD (mask scale) change as a function of defect size for several mask focus positions. All defects are 50- 60nm FWHM and centered in the space between dense 250nm absorber lines 55nm from the edge of the absorber

3. RADICAL SIMULATION OF 22NM AND 16NM NODES

RADICAL will now be used in advance of availability of high volume manufacturing quality exposure tools, resists, and masks to assess the expected defect printability levels in less coherent, production conditions. In this work it is assumed that a defect causing a 10% or larger change in space CD is unacceptable.

The multilayer geometries used in this simulation work assume the multilayer smoothing described in [8] is used to grow the multilayer stack. This process tends to lower the height of the defect for each layer deposited and causes the surface width to either increase or decrease to 50-100nm FWHM.

Simulation conditions

The model assumed a prototypical EUV scanner to print 22nm and 16nm dense lines is a 4x system with an NA of 0.32. This corresponds to a k1 of about 0.5. Here, either top-hat or annular illumination might be used. To emphasize the need for a high collection illuminator efficiency, a top-hat illumination system with sigma of 0.75 has been chosen for the first part of this work. The results will change if off-axis illuminations, like annular or dipole are used, which will be demonstrated.

The 13.5nm light is incident on the mask at an angle of 6°. This incident light is perpendicular to the line space patterns simulated, causing shadowing and other effects on the final image.

Critical dimension (CD) will be calculated with a constant threshold resist model. The threshold was chosen as the value that gives the nominal CD, in this case 22nm, at best focus with no defect present. The size and position of the buried defect relative to the 88nm dense lines on the mask will be varied. A summary of the buried defect sizes used in these simulations, along with the resulting surface defect sizes, is given in Table 2.

Buried Height	Buried Width	Surface Height	Surface Width
1.3	50	0.4	75
2.5	50	0.8	74
5	50	1.4	73
10	50	2.2	72
15	50	2.8	72

Table 2. Sizes of defects simulated in RADICAL on the substrate and on the surface of the mutlilayer. All sizes are in nm. All widths are FWHM.

Effect of Defect Position

As described in [4], RADICAL's design makes simulating several different absorber patterns over the same defect fast and easy. Therefore, all investigations in this work will simulate the effect of a defect as a function of position across an entire period on the mask. The resulting CD change as a function of position for several defects is shown in Figure 4.

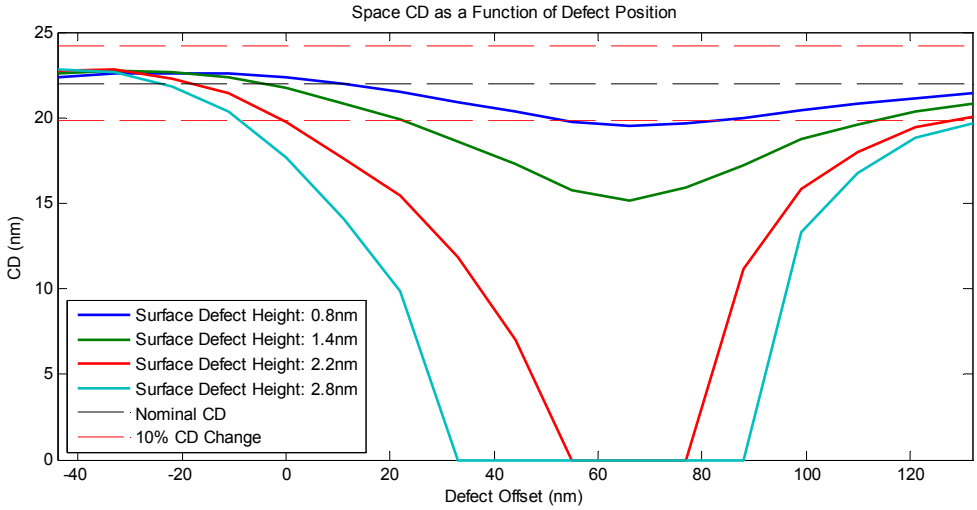

Figure 4. Space CD of 22nm dense lines as a function of defect position for multiple defect sizes and tophat illumination with a partial coherence of σ=0.75.

Several interesting conclusions can be drawn from these results. The first is that a 2.2nm tall defect will cause resist bridging if it is located anywhere between 55nm and 75nm from the absorber edge. This is the worst case area in which a defect can be located. However, in practice many defects that do not cause feature bridging will still not be acceptable because tolerable CD change due to a defect is actually a small percentage of the space width. For this work, 10% will be used as the maximum allowable space CD change. The RADICAL simulations in Figure 4 show that a defect as small as 0.8nm will cause a 10% CD change if it is located 65nm from the edge of the absorber line. This means if a mask blank has no defects taller than 0.8nm it can be relied on for EUV printing of 22nm dense lines, assuming no focus variation.

Figure 4 is not symmetric due to the 6° incident angle of the EUV light. For negative offsets, the size of the space is actually increased by the defect and for positive offsets the space width is reduced. Also, all of the curves in Figure 4 are shifted right due to the 6° incident angle. For normally incident light, the curves would be symmetric around an offset of +44nm, where the defect is centered in the space. But, in Figure 4 the curves are roughly symmetric around an offset of +66nm, 22nm different than the expectation for normal incidence. The absorber stack in these simulations was 87nm tall, 75nm of TaN and 12nm of an anti-reflection coating for mask inspection. A simple geometric ray tracing calculation of the round trip shadowing distance predicts a horizontal displacement of 18nm from the normal incidence case. This is close to the value of 22nm observed in simulation, suggesting geometric approximations are a good first pass method for predicting shadowing effects. But, the most important conclusions regarding shadowing is that when considering the effect of a defect, its position and the angle of the incident light must be considered together.

Figure 5 shows the results for 16nm dense lines. All of the characteristics of the 22nm results are present in the 16nm results, but the sensitivity to defects is increased greatly. This is due mainly to the reduced image slope from 22nm to 16nm patterns.

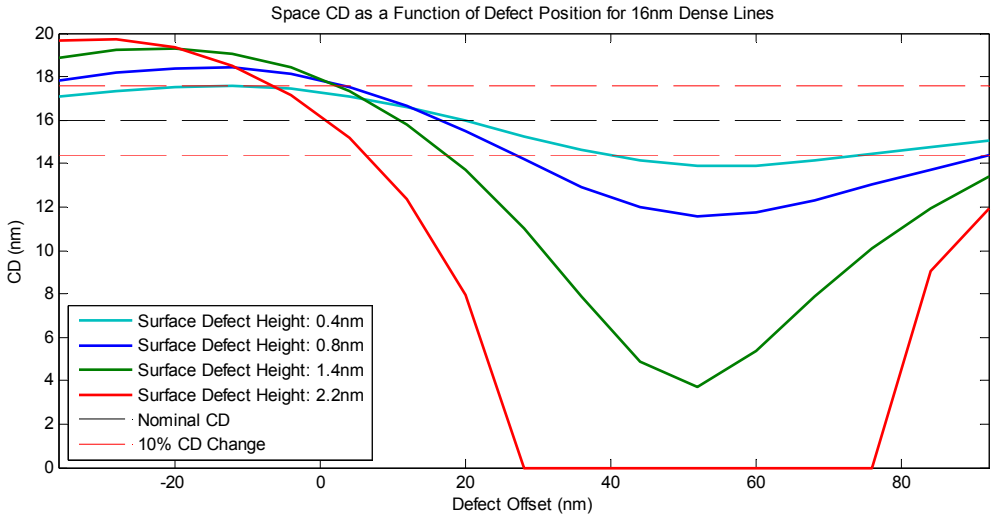

Figure 5. Critical dimension of 16nm dense lines as a function of defect position for multiple defect sizes and tophat illumination with a partial coherence of σ=0.75.

Effect of Focus

The analysis in [7] shows the clear effect of focus on buried EUV defects. Both RADICAL simulations and AIT images of isolated buried defects invert their center intensity through focus. The center intensity of the aerial image of an isolated bump defect is below the clear field value for negative focus, which is defined as moving the wafer away from the lens, and above the clear field value for positive focus. This effect is shown in Figure 6, which compares through simulation the center intensity of three defects: a thin mask square magnitude defect, a thin mask square uniform phase defect and a buried EUV defect.

This inversion through focus is apparent in the images of buried defects near features as well. Figure 7 shows the resulting space CD for nominally 22nm lines as a function of the position of 0.8nm tall defect for three focus values.

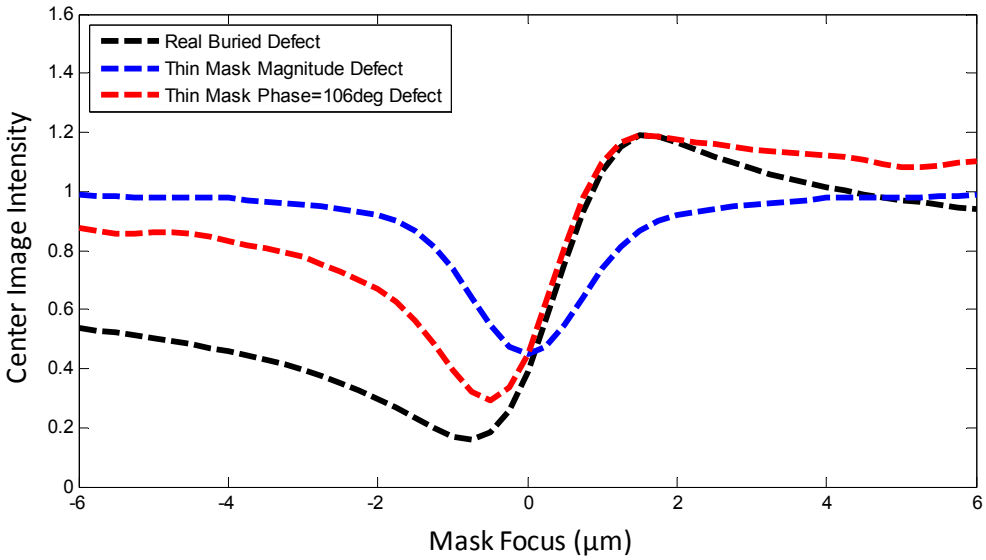

Figure 6. Simulated center intensity of the aerial image of three isolated defects as a function of focus for tophat illumination with σ=0.75.

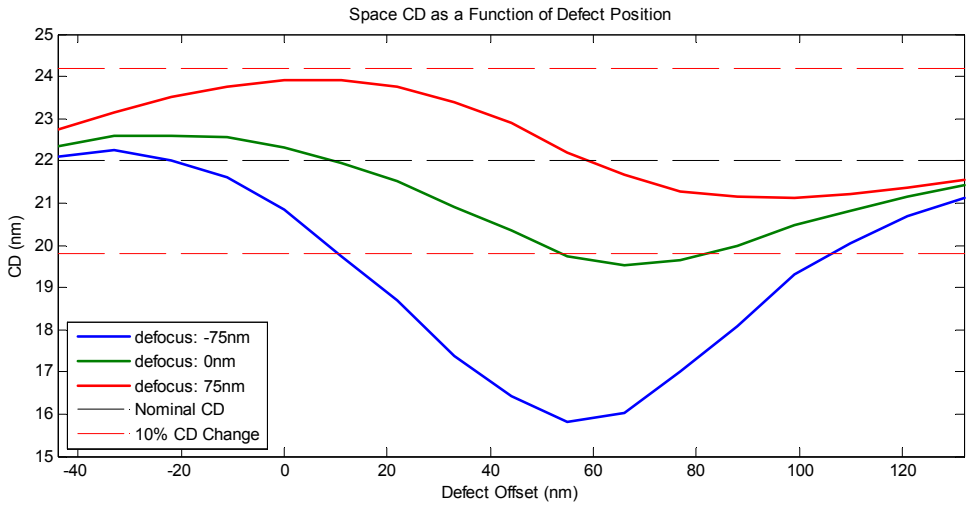

Figure 7. CD for 22nm lines as a function of the position of 0.8nm tall defect for three focus values

Figure 7 shows that for negative focus the space CD is decreased and for positive focus the space CD is increased. This is consistent with Figure 6, where the defect is brighter for positive focus and darker for negative focus. There are a few interesting offset locations to note. From 15nm to 50nm offset, the CD change is within the 10% boundary at best focus, but out of focus it is beyond the limit. This shows that focus must be considered when minimum defect sizes are defined. The other interesting position is at 10nm offset, where there is no CD change due to the defect in focus, but out of focus the CD change is nearly 10%. This shows that inspection through focus may be necessary for defect detection.

Effect of Illumination

The previous sections have shown that reduced image slope and variation in focus position can make defects more printable. It has been shown experimentally that defect printability does depend on illumination [5]. It turns out that the problem of image slope could be reduced by changing the illumination. Reduction in through focus defect printability is not as simple to achieve.

The improvement of image slope and contrast with off-axis illumination is well established. Figure 8 shows the contrast values predicted by RADICAL for 22nm and 16nm dense lines. The 16nm case is more improved by the dipole and annular illuminations, so it will be the focus of this section.

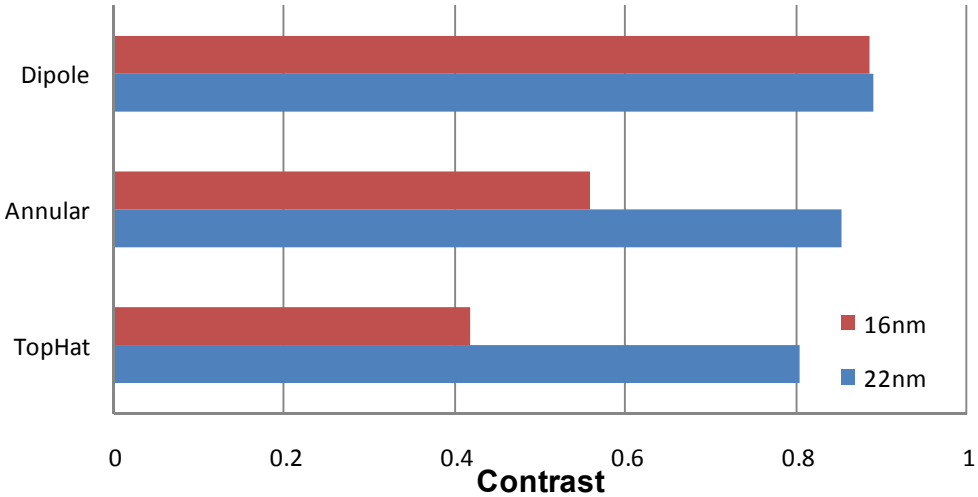

Figure 8. Contrast of the aerial images of 22nm and 16nm dense line patterns with three illuminations.

The image of an isolated buried defect is strongly dependent on the illumination. Figure 9 shows the center intensity of a buried defect for the three types of illumination, with the dipole and annular illuminations optimized for printing 16nm line space patterns. The inversion of the center intensity does not occur with annular and dipole illumination. Also, the minimum intensity, around -75nm defocus, does not appear to be as bad for these illuminations as it is for tophat. Although the center intensity values are nearly identical for annular and dipole illuminations, it is important to note that the images are quite different, as shown in Figure 10.

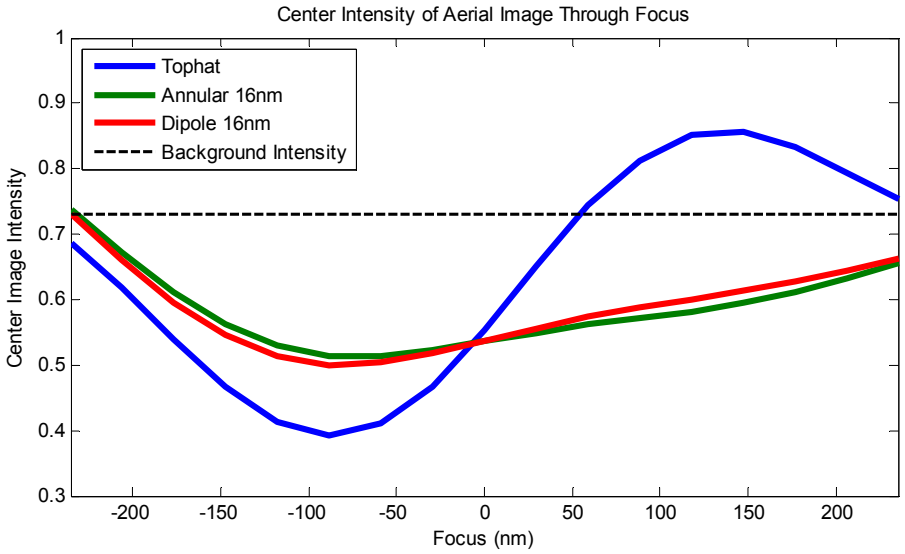

Figure 9. Center intensity of the aerial image a buried defect as a function of wafer focus level for three illuminations

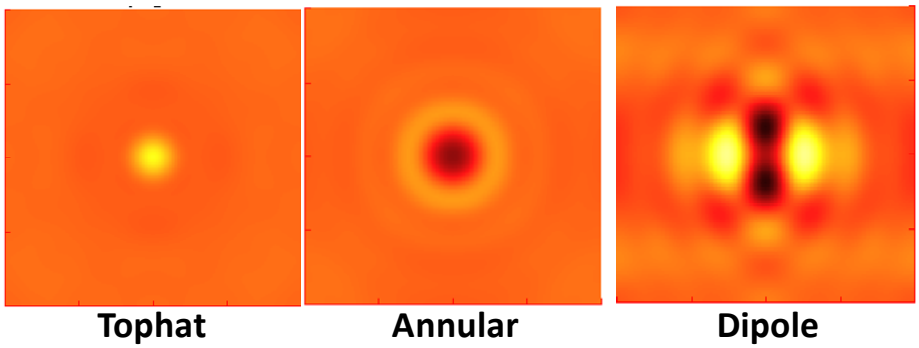

Figure 10. Image of isolated buried defect at +125nm defocus for three illuminations

The reduction of defect printability for annular and dipole illuminations is shown in Figure 11 for best focus. The reduction in sensitivity seems to follow the same trend as the increase in contrast, suggesting that a way to decrease defect printability is to increase contrast.

Through focus, however, the off-axis illuminations do not always reduce defect printability. As Figure 12 shows, the defect has a more complicated effect for annular and dipole illuminations through focus than it does for tophat. The space containing the defect with tophat simply expands and contracts near the defect through focus, as expected from the previous results in the paper. But, the annular and dipole illuminations cause the defect to affect a larger area of the image. The dipole image is particularly interesting. In focus, the image appears to be defect free. But, for positive defocus the space CD is decreased above and below the defect and increase to the left and ride of the defect. This is what the isolated image of the defect in Figure 10 suggests. The effect is opposite for negative focus.

For annular illumination, similar effects over a large area are observed, but the magnitude of the changes due to the defect is much smaller. This suggests that annular illumination may be the best illumination for printing 16nm dense lines that are insensitive to defects through focus. The mutual intensity function for each illumination is also shown in Figure 12. The dark areas of the mutual intensity function show the points where there is no interaction with the fields from the center point. The orange areas show positive interaction and the blue areas show negative interaction. The

dipole mutual intensity function shows that the defect interacts strongly over the entire domain, so the effects observed in the aerial image plots are not surprising.

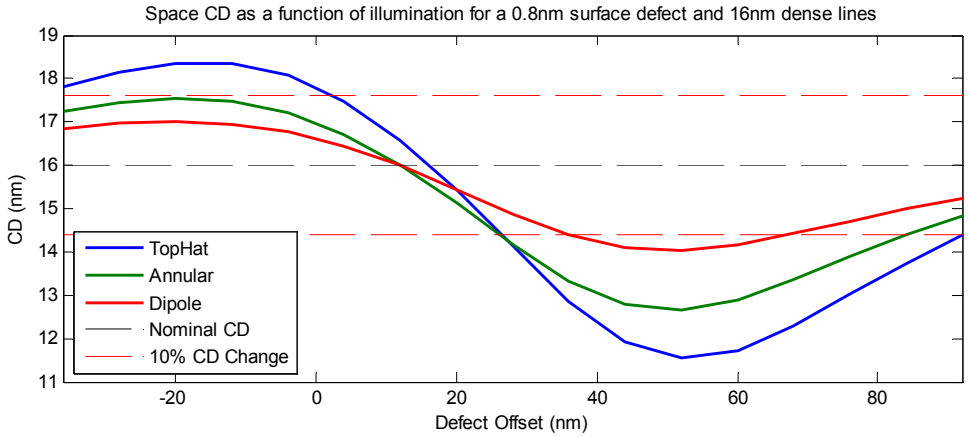

Figure 11. CD for 16nm lines as a function of the position of 0.8nm tall defect for three types of illumination.

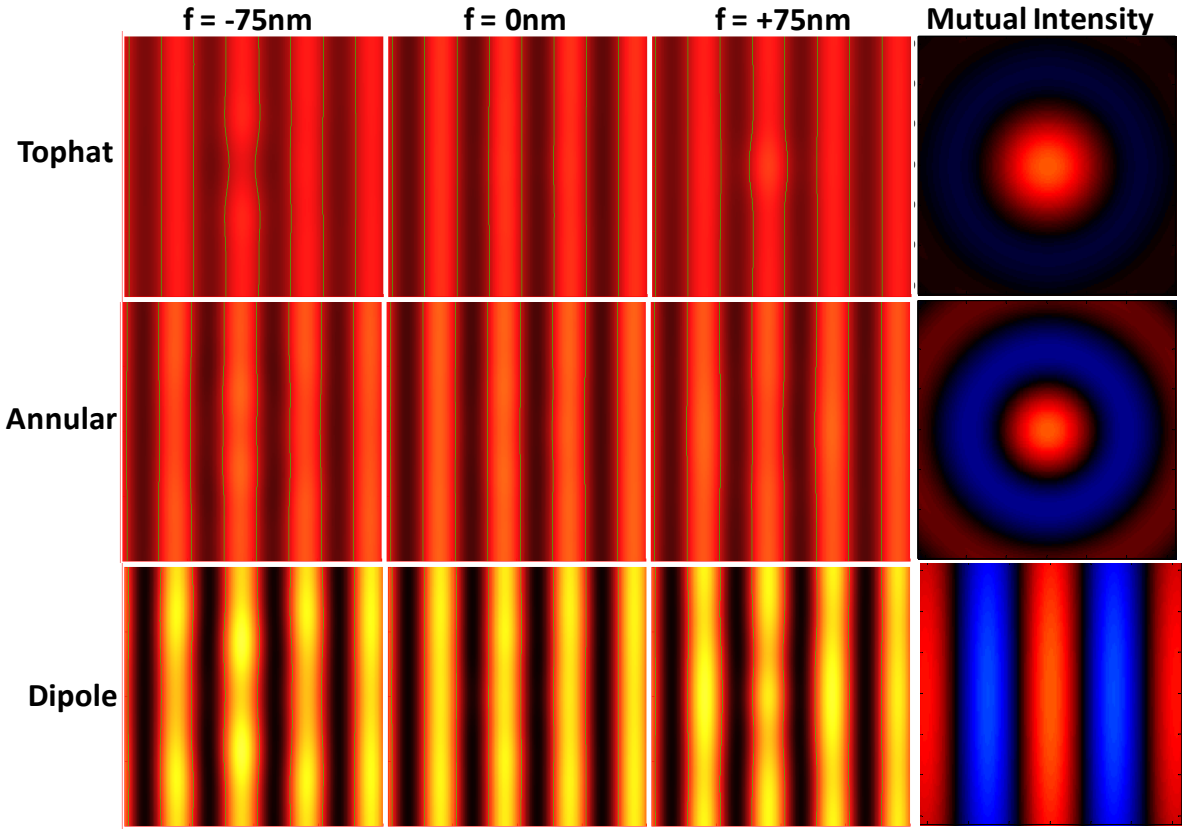

Figure 12. Aerial images through focus for three illuminations of a 0.8nm defect 16nm (mask scale) the edge of an absorber line in a 16nm (wafer scale) dense line space pattern. The mutual intensity function for each illumination is also shown. The physical size for all plots is 128nm x 128nm wafer scale.

Comparison to ITRS Roadmap

The International Technology Roadmap for Semiconductors (ITRS) sets limits for nearly every aspect of semiconductor manufacturing, including the size of EUV mask defects [9]. It specifically addresses opaque defects and substrate defects, but these specifications do not capture the the types of defects discussed above: bumps on the substrate that cause very short but wide multilayer surface bumps. According to the 2008 ITRS for 23nm Flash half-pitch, for example, the allowable opaque defect size, defined as the sqaure root of the area, is 23nm. The substrate defect size, defined as the diameter of a spherical defect, is 30nm. It is not clear that either of these specifications would disallow the critical defect for 22nm lines in focus: 0.8nm tall and 74nm FWHM. A multilayer bump is not an opaque defect, so even though it is much larger than the 23nm limit it would not be covered by that specification. A multilayer bump is usually caused by a substrate defect, but it is not clear how the substrate specification translates to the surface bump. The relationship between a substrate defect and a surface defect is determined by the deposition process, which is different for each blank manufacturer. It is clear that for the ITRS roadmap to fully specify the EUV mask defect limits, it will need to mention the allowable surface height and width for bumps on the surface of the multilayer. Commercial mask inspection tools will also be needed to detect these small defects on an EUV mask. The AIT is able to detect defects well below 1nm tall, but it is a research tool. There are currently no commercial tools which are able to detect defects this small on a patterned EUV mask.

4. CONCLUSION

Buried defects in EUV masks are still a major road block to the implementation of EUV lithography. The two major problems discussed in this paper are mask inspection and defect printability. The first section showed that the Actinic Inspection Tool is able to detect defects below 1nm tall on the multilayer surface. This is approximately the sensitivity that will be required for 22nm dense lines. Unfortunately, the AIT is a research tool which does not meet high volume manufacturing mask inspection throughput requirements. The AIT results also demonstrated the effect of defects through focus, especially the decrease in space CD in the presence of a bump defect for negative focus.

RADICAL was used to show the effects of defects near features for 22nm and 16nm lines, because no defectivity experiments have been done yet for features of this size. The maximum allowable defect size for a 10% CD change in focus was 0.8nm for 22nm lines and 0.4nm for 16nm lines if a tophat illumination is used. The linewidth is shown to be more sensitive to buried defects out of focus, but less sensitive to defects if annular or dipole illumination is used in focus. Through focus, annular and dipole illuminations cause the defect to affect a larger area and do not always result in a reduction in defect printability over tophat illumination. This sensitivity to short wide defects on the multilayer surface is not currently represented in the EUV mask defect specification of the ITRS roadmap.

[1] Conclusion of Steering Committee at the 2008 International Symposium on Extreme Ultraviolet Lithography

[2] K. A. Goldberg, P. Naulleau, I. Mochi, E. H. Anderson, S. B. Rekawa, C. D. Kemp, and R. F. Gunion, H.-S. Han, S. Huh, "Actinic extreme ultraviolet mask inspection beyond 0.25 numerical aperture," *J. Vac. Sci. & Technol*. B 26 (6), 2220-4 (2008).

[3] K. A. Goldberg, I. Mochi, S. Huh , "Collecting EUV mask images through focus by wavelength tuning," *Proceedings of SPIE*, Vol. 7271 (2009).

[4] C. H. Clifford, A. R. Neureuther, "Fast simulation methods and modeling for extreme ultraviolet masks with buried defects", *J. Micro/Nanolith. MEMS MOEMS* 8, 031402 (2009).

[5] T. Liang, et al, "Growth and printability of multilayer phase defects on extreme ultraviolet mask blanks," *J. Vac. Sci. Technol.* B25 (6), 2098 (2007) .

[6] Clifford, C. H., et al. "Smoothing based fast model for images of isolated buried EUV multilayer defects," *Proceedings of SPIE*, Vol. 6921, (2008).

[7] C. H. Clifford, S. Wiraatmadja, T. T. Chan, A. R. Neureuther, K. A. Goldberg, I. Mochi, T. Liang, "Comparison of fast 3D simulation and actinic inspection for EUV masks with buried defects," *Proceedings of SPIE*, Vol. 7271, (2009).

[8] D. G. Stearns, P. B. Mirkarimi. and E. Spiller, "Localized defects in multilayer coatings," *Thin Solid Films* 446(1), 37–49 (2004).

[9] The International Technology Roadmap for Semiconductors, 2008 Update.